Bioengineered-Inorganic Nanosystems for Nanophotonics and Bio-Nanotechnology

Kirsty Leong[a], Melvin T. Zin[b], Hong Ma[b], Fei Huang[b], Memet Sarikaya[b], Alex K.-Y. Jen[*a,b]
[a]Department of Chemistry, University of Washington, Seattle, [b]Department of Material Science and Engineering, University of Washington, Seattle, WA USA 98195

ABSTRACT

Here we nanoengineered tunable quantum dot and cationic conjugated polymer nanoarrays based on surface plasmon enhanced fluorescence where we achieved a 15-fold and 25-fold increase in their emission intensities, respectively. These peptide mediated hybrid systems were fabricated by horizontally tuning the localized surface plasmon resonance of gold nanoarrays and laterally tuning the distance of the fluorophore from the metal surface. This approach permits a comprehensive control both laterally (i.e., lithographically defined gold nanoarrays) and vertically (i.e., QD/CCP-metal distance) of the collectively behaving QD-NP and CP-NP assemblies by way of biomolecular recognition. The highest photoluminescence was achieved when the quantum dots and cationic conjugated polymers were self-assembled at a distance of 16.00 nm and 18.50 nm from the metal surface, respectively. Specifically, we demonstrated the spectral tuning of plasmon resonant metal nanoarrays and the self-assembly of protein-functionalized QDs/CCPs in a step-wise fashion with a concomitant incremental increase in separation from the metal surface through biotin-streptavidin spacer units. These well-controlled self-assembled patterned arrays provide highly organized architectures for improving opto-electronic devices and/or increasing the sensitivity of bio-chemical sensors.

Keywords: hybrid nanosystem, surface plasmon enhanced fluorescence, quantum dots, conjugated polymers,

1. INTRODUCTION

Growing interest in the use of bio-nanomaterials for more efficient opto-electronic devices and more sensitive biosensors has paved the way to develop better design systems. These systems have increasing been a coordination between materials science and biological sciences on the nanometer scale.[1] Hybrid nanoassemblies made from inorganic nanostructures and biological molecules serve as versatile nanocomposites with a range of surface functionalities as well as optical and electronic properties that arise from co-operative interactions.[2a] Of peculiar utility in nanobiotechnology is the integrated system of designed peptides/proteins, metal nanoparticles, and semiconductor nanocrystals.[2b]

In recent years, hybrid nanosystems composed from metals such as gold or silver nanostructures and organic fluorophores or semiconductor nanocrystal (typically CdSe or CdSe-Zn) quantum dots (QDs) have been thoroughly investigated.[3] These hybrid systems focus on using surface plasmons in metal nanostructures to alter the electronic properties of their surrounding environment. Upon the excitation of light, gold and silver nanoparticles display an enhanced electric field (E) near the particle surface such that $|E^2|$ can be 100-10,000 times greater in intensity than the incident field.[4] The use of metallic nanostructures can modify the spectral properties of the fluorophore, and therefore alleviate some of its physical constraints. The fundamental importance and interest in the fabrication of nanomaterials lies in the ability to precisely modify the electronic states of fluorophores or QDs. By using surface plasmons to modify the electronic states of fluorophores, the performance, sensitivity, and response time of a system can be enhanced, a phenomena known as metal enhanced fluorescence.

Metal enhanced fluorescence (MEF) is a powerful technology influenced by near-field interactions of a fluorophore with metal nanostructures.[5] The proximity of fluorophores with metal nanostructures can result in either a dramatic increase or quenching of the fluorophore's emission and extent of resonance energy transfer.[6] This interaction is known to affect the emission of nearby fluorophores by several mechanisms: enhanced excitation and increased radiative decay rates, photostability, and quantum yield. The size similarities between metal nanostructures and

* Further author information: (Send correspondence to A.J.)

A.J.: E-mail: ajen@u.washington.edu, Telephone: 1 206 543-2626; fax 1 206 543-3100

Nanobiosystems: Processing, Characterization, and Applications, edited by Emily M. Heckman, Thokchom Birendra Singh, Junichi Yoshida, Proc. of SPIE Vol. 7040, 704007, (2008) · 0277-786X/08/$18 · doi: 10.1117/12.801490

biomolecules and the ability of metal nanostructures to bond chemical species make them desirable tools for highly sensitive detection. The excitement of plasmonics lies in its potential to achieve highly miniaturized and sensitive photonic devices by controlling, manipulating, and amplifying light on the nanometer length scale.[7]

Similarly to the tunable optical properties of nanoparticles, the photoluminescence of QDs can be tuned by controlling their size. QDs are semiconductor nanocrystalline clusters with sizes ranging in a few nanometers. They have exceptional photochemical stability, high quantum yield, size tunable emission spectra with a narrow emission bandwidth, and a broad excitation.[8] The unique optical properties of QDs makes them more desirable fluorophores for applications compared to organic dyes.

In the second part of this study, we introduce another unique class of material known as conjugated polymers. The transport, electrical conductivity, and amplifying properties of conjugated polymers (CPs) offer a myriad of opportunities to couple analyte receptor interactions into observable responses.[9] The delocalized electronic structure of CPs can be used as highly responsive optical reporters for chemical and biological targets. Because the effective conjugation length is substantially shorter than the number of repeating units, the backbone serves to hold a series of conjugated segments in close proximity.[10] Thus, CPs are efficient for light harvesting and enable optical amplification. When coupled with gold nanostructures, conjugated polymers can offer higher sensitivity compared to organic fluorophores and biocompatibility due to an increase in the electromagnetic fields and its electrical charge. Thus, it is our interest to investigate the effects of metal nanostructures on the optical properties of cationic conjugated polymers (CCPs).

Here, we developed a protein-enabled strategy to fabricate tunable QD and cationic conjugated polymer (CCPs) nanoarrays where up to 16-fold and 25-fold increase in the surface-plasmon-enhanced photoluminescence has been achieved, respectively. This result, to the best of our knowledge, represents the highest fluorescence enhancement from hybrid nanostructures based on biomolecules. We demonstrate the spectral tuning of plasmon resonant metal nanoarrays and the self-assembly of protein-functionalized QDs and CCPs in a step-wise fashion with a concomitant incremental increase in separation from the metal surface through biotin-streptavidin spacer units. This approach, therefore, permits a comprehensive control both laterally (i.e., lithographically defined gold nanoarrays) and vertically (i.e., QD-metal distance) of the collectively behaving QD-NP and CCP-NP assemblies by way of biomolecular recognition. As a result, we were able to correlate emission as a function of QD and CCP-metal distance and resonant spectra. In contrast to molecular beacon-style assays,[11] the use of a nanopatterned substrate allows the QD and CCP probes to be employed in an array format for possible incorporation into lab-on-chip applications[12] and also provide additional discrimination between surface-bound and free fluorophores by increasing emission under evanescent wave excitation.[13]

2. METHODOLOGY

2.1 Materials and Substrates

Boron-doped Si(100) wafers of test-grade (diameter: 100 mm; resistivity: 1-10 Ω/cm; thickness: 525 ≠ 50 μm) were purchased from Silicon Sense (Nashua, NH). All reagents and solvents, and salmon DNA were obtained from Sigma-Aldrich (St. Louis, MO) and used as received unless otherwise stated. Deionized water used for rinsing samples was produced with a NANOpure Diamond^{TM} purification unit (Barnstead International, Dubuque, IA) and had a resistivity of ~15 MΩ cm^{-1}.

A short interlinker, 1-4-dibiotinylbutane, consists of two biotin groups at opposite ends for holding multiple layers of streptavidin molecules and was synthesized in-house in our laboratory. It was dissolved in absolute (200 proof) ethanol (Aaper Alcohol and Chemical Company, Shelbyville, KY) to a concentration of 1.0mM. Streptavidin was purchased from Sigma-Aldrich (St. Louis, MO) and dissolved in deionized water to a concentration of 1.0mM without further purification.

A cationic conjugated polymer, poly[(9,9-bis(6'-((N,N,N-trimethylammonium)hexyl)-2,7-fluorene)-co-4,7-di-2-thienyl-2,1,3-benzothiadiazole] dibromide (PFDBT-N^+), was synthesized in-house in our laboratory. The absorbance maximum is at 380 nm. The emission maximum is at 620 nm. It was dissolved in 10% methanol and water to a concentration of 0.1 mg/mL. The chemical structure is shown in figure 1.

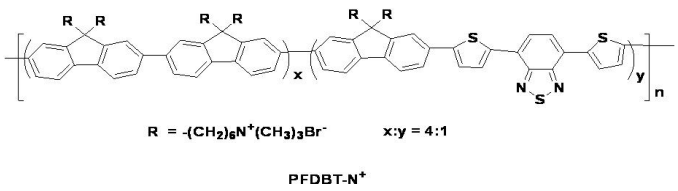

Fig. 1. Chemical structure of the cationic conjugated polymer, poly[(9,9-bis(6'-((N,N,N-trimethylammonium)hexyl)-2,7-fluorene)-co-4,7-di-2-thienyl-2,1,3-benzothiadiazole] dibromide (PFDBT-N^+). Absorption maximum at ≈ 380 nm. Emission maxima at ≈ 620 nm.

Biotinylated gold binding polypeptide (bio-AuBP2L), a 12 amino acid peptide sequence, was synthesized by Sarikaya lab. The concentration of the peptide solution was 100 μg/mL and prepared in a phosphate buffer (3:1 K_2HPO_4:KH_2PO_4) solution containing 10 mM potassium phosphate and 100 mM potassium chloride (ca. pH 7.2 without further adjustment).

Biotin functionalized CdSe-ZnS core-shell quantum dots were acquired from Invitrogen Corp. (Carlsbad, CA). They have an absorption maximum at 595nm and an emission maximum at 605 nm. The QD 605 biotin conjugate stock solution (2 μM) was diluted to a concentration of $1.0x10^{-8}$ M in phosphate buffer solution prepared as above for AuBP2L.

2.2 Fabrication of gold nanoarrays

Electron-beam lithography was performed using a field emission scanning electron microscope (SEM; FEI Sirion, Hillsboro, OR) that has been equipped a nanolithography system. Nanometer Pattern Generation System (NPGS), developed by JC Nabity Lithography System (Bozeman, MT), was used to design and direct-write the nanoarrays. The resolution of the nanolithography system is approximately 20 nm. Prior to EBL, Si wafers were fractured into 1 x 1 cm^2 substrates and cleaned in a two-step procedure: (i) piranha etch, 3:1 H_2SO_4:H_2O_2(30%) for 1 hr; (ii) base treatment, 5:1:1 H_2O:NH_4OH:H_2O_2(30%) with sonication for 1 hr. Thin films (50 – 80 nm) of PMMA (950k; diluted in chlorobenzene) positive resist were spin-coated on Si (001) substrates, annealed at 180 ^OC on a hot plate for 2 min to improve the film uniformity, and were exposed to an electron beam at an accelerating voltage of 30 keV. After the electron-beam exposure, the samples were developed in a 1:3 mixture of methyl-isobutylketone/proponol (MIBK/IPA) at room temperature for ~ 30 sec and baked at 90 ^OC in a vacuum oven for 30 min. The samples were checked by SEM to assess the integrity of nano-patterned PMMA films before the metallization process.

Metal was deposited onto nano-patterned PMMA films by electron-beam evaporation (SEC 6000, CHA Industries) under a high vacuum with base pressure of ~ 1 x 10^{-6} torr. For stronger adhesion of gold to silicon, 1 nm of chromium was used. The deposited thickness and deposition rate were measured by a quartz crystal microbalance (QCM). The deposition rate was maintained at ~ 0.1 nm/s to achieve high-quality gold nanostructures with smooth surfaces. In the lift-off step, gold nanoarrays were obtained by dissolving the PMMA in acetone overnight (~ 12 hr). To ensure a complete removal of PMMA, the samples were treated as follows: (i) thorough rinsing in acetone and IPA; (ii) brief immersion in a piranha solution for 3 min; (ii) oxygen plasma etch for 30 min. It is critical that PMMA is entirely stripped from the substrate in order for the molecular linkers to self-assemble specifically onto the metal nanoarrays. Empirical evidence suggests that PMMA interferes with the self-assembly protocol by binding with peptides and streptavidin molecules, presumably through van der Waals and electrostatic interactions. This often leads to non-specific adsorption of molecular linkers.

2.3 Assembly of molecular linkers

The assembly protocol begins with the binding of biotinylated gold binding polypeptide (bio-AuBP2L) onto gold nanoarrays, followed by sequential attachment of spacer units made of strepavidin and 1-4-dibiotinylbutane. Samples (~ 1 x 1 cm^2) are immersed into 2 mL solutions of their respective molecular linkers for a specific duration. Immobilization of bio-AuBP2L onto gold nanoarrays was performed for 2 hr to ensure a uniform well-packed foundation layer. Sequential layer-by-layer assemblies of streptavidin and 1-2-dibiotinylbutane molecular linkers were under a reaction time of 60 mins between each attachment. Careful and thorough rinsing, ~ 3 mins with PBS and ~ 3 mins with deionized water and gentle ultra-sonication in water ~ 1 min, was performed after each step to ensure complete removal of excess molecular linkers to accomplish reproducible spacer units at well-defined lengths. The presence of residual

molecular linkers from a previous step detrimentally affects the subsequent step by lowering the efficiency of specific binding.

2.4 Assembly of Cd/Se ZnS quantum dots

Streptavidin functionalized quantum dots were attached onto dibiotin linkers through biotin-streptavidin interaction. The sample was positioned in a Petri dish and incubated for 30 mins with 20 uL of the working QDs solution (1.0×10^{-8} M) onto a nano-patterned area (10×10 um^2) on the substrate. Control samples used for comparison of both Au and glass substrates, the sample volume of QD solutions was pipetted onto a region of the substrate of equal surface area. During the QD assembly, a few droplets of deionized water were placed inside the Petri dish to prevent the evaporation of the QD solution and the lid was closed. This minimizes minor changes in the local concentration of the QD solution.

2.5 Assembly of cationic conjugated polymers

Biotinylated gold-binding polypeptide (bio-AuBP2L) is attached onto the functionalized gold nanoarrays for 1 hr. The cationic functionality of gold-binding polypeptide allows for the subsequent attachment of the negatively charged phosphate backbone of DNA via electrostatic interactions. A 50 µl solution of 2 mg/mL of salmon DNA is placed onto the functionalized gold substrate and is allowed to self-assemble for 20 mins. The substrate is rinse thoroughly for 5 mins in PBS buffer and DI water to ensure a monolayer of DNA. Then 50 µl of 2 mg/mL of cationic conjugated polymers is placed onto the substrate and the polymer is allowed to self-assemble for 20 mins onto DNA through electrostatic interaction. The substrate is once again washed with PBS buffer and DI water to ensure unbound and loosely bound molecules are removed.

2.6 Optical microscopy and spectroscopy

Optical microscopy and spectroscopy were performed using a Nikon TE-2000 inverted microscope fitted with a transmitted darkfield condenser and a 50X objective (Nikon Plan RT, NA 0.7, CC 0-1.2) with an intermediate 1.5X lens (total magnification 75X). The microscope output was either directed to a thermoelectrically-cooled color CCD camera (Diagnostic Instruments, FX1520) or a fiber optic cable (diameter = 200 µm, UV-vis transmission, Ocean Optics, Dunedin, FL) coupled to a portable charge coupled device spectrometer (USB2000, Ocean Optics). A standard tungsten halogen lamp was used for transmitted light darkfield illumination, and metal halide lamp (EXFO X-Cite 120) was used for epi-fluorescence illumination.

The fluorescence spectra were obtained via epi-fluorescence thru a 405 ± 10 nm short bandpass excitation filter or a 360 ± 10 nm short bandpass excitation, a 520 dichroic mirror, and a 560 longpass emission filter for QDs and CCPs. The filters were purchased from Chroma Technology Corp (Rockingham, VT), reduced scattered and/background signal. To check for homogeneity and reproducibility of QD emission and CCP emission, samples were mounted on a stage and the PL spectra were acquired in 1 µm step within each pattern.

3. RESULTS

Using electron-beam lithography (EBL), we fabricated nine unique geometric arrangements of gold nanoarrays for plasmonic coupling with QDs and cationic conjugated polymers (CCPs), shown in figure 2. Gold metal was chosen because of its stability and strong scattering of light in the visible frequencies. In addition, it allowed for the specific adsorption of AuBP2L. Gold nanopillars of 3 sizes (D = 50, 100, 200 nm) were periodically ordered at 4 grating constants (d_{tt} = 50, 100, 150, 200 nm) while the height was kept constant (h = 50 nm). Each pattern occupied a 10 x 10 µm^2 and was repeated three times to ensure reproducibility and to acquire a larger data set. All patterns were fabricated on the same sample. These plasmon resonant metal nanoarrays exhibited distinct light scattering properties shown in figure 3. This is accomplished by systematically varying their size and grating constant thereby controlling their absorption cross-sections,[12] as confirmed by scattering spectral measurements.[14]

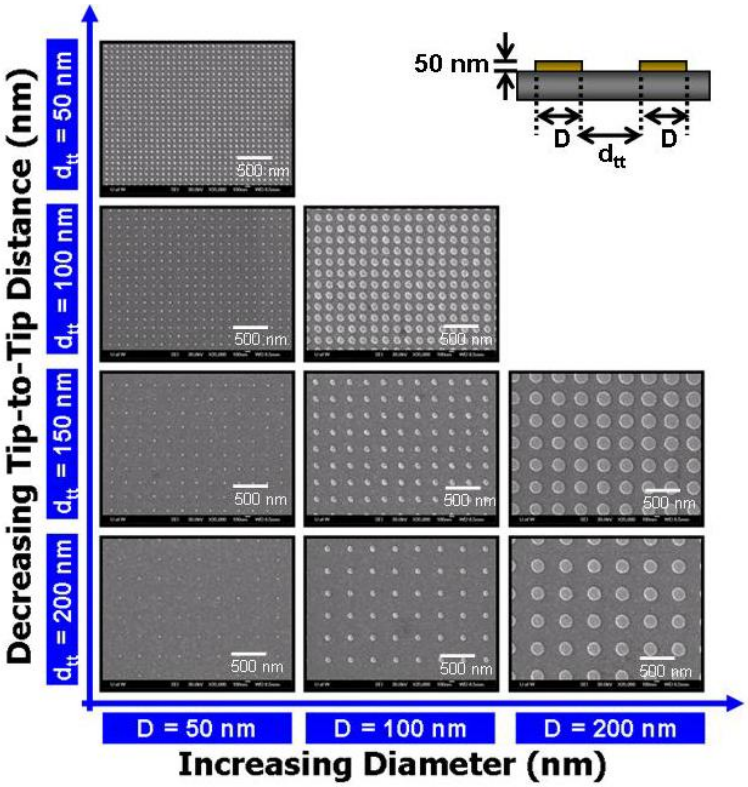

Fig. 2. SEM images of gold nanoarrays. EBL readily allows the precise control of the size and interspacing of gold nanopillars, which is ideal for spectral tuning of the LSPR of metal nanostructures and studying their electromagnetic interactions. By keeping the height constant (h = 50 nm), gold nanopillars of 3 sizes (D = 50, 100, 200 nm) were periodically ordered at 4 grating constants (d_{tt} = 200, 150, 100, 50) to produce 9 unique arrangements. Each pattern occupied 10 x 10 μm^2 and was repeated 3 times to ensure reproducibility and acquire a larger data set. All patterns were fabricated on the same sample.

Plasmon excitations in metal nanoparticles produced extinction spectra that depend sensitively on their size, shape, material, and dielectric environment. In the case of neighboring nanoparticles such as these periodically ordered metal nanopillars, electromagnetic interaction between neighboring nanostructures in these periodically ordered metal nanopillars was often complicated by the extinction spectra because higher modes of plasmon excitation occurred.[15] Typically, two types of optical communication can be distinguished in a regular 2-D configuration: near-field coupling and far-field dipolar interaction. Near-field coupling was more dominant and relevant for 50 nm arrays because of the short range of EM near-fields in the order of tens of nm. Far-field dipolar interactions were mediated through scattered light which is of dipolar nature for sub-wavelength nanostructures and can be described within a quasi-static model.[15] This light-matter interaction manifested in spectral scattering of light as demonstrated in the true-color dark field images of metal nanoarrays (Figure 3). In the case of where d_{tt} is too large to allow near-field coupling, these metal nanopillars radiated via interfering dipolar fields.[16]

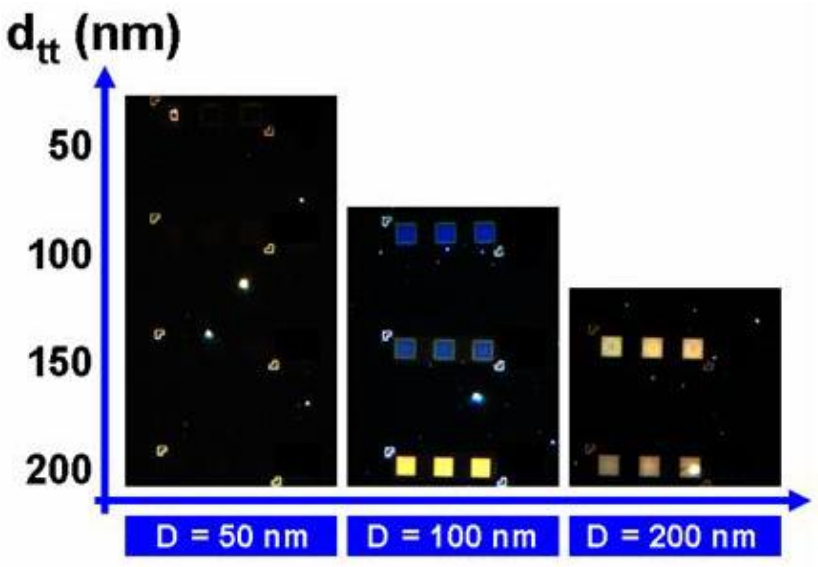

Fig. 3. Scattering image of gold nanoarrays. Precise control of the size and interspacing of gold nanopillars leads to metal nanoarrays with distinct light scattering properties.

We calculated the LSPR maxima (λ_{max}) of metal nanoarrays by calculating their scattering efficiency (Table 1). These calculations showed that the optical properties of 200 nm pillars was independent of tip-to-tip spacig at d_{tt} = 150, 200 nm which suggested weak EM interaction between large nanostructures which was not significantly smaller than the wavelength of light (i.e. beyond quasi-static limit). For 100 nm metal nanoarrays, the opposite effects were observed. The resonant wavelength blueshifted as the tip-to-tip spacing decreased. For 50 nm metal nanoarrays, the scattered light did not occur in the visible frequencies. The extinction peaks of gold metal nanoarrays with small tip-to-tip spacing (relative to their size) red-shifted to IR frequencies. Thus we observed the effects of radiative dipolar interactions (which has a 1/d dependence on nanoparticle separation) and retardation (which multiplies the dipole field by e^{ikd}) for large grating constants (d_{tt} = 100, 150, 200 nm).

Table 1. Structural parameter and optical properties of gold nanoarrays.

Pattern	Nanostructure Dimensions		Area Fill Factor	LSPR Peak
	D (nm)	d_{tt} (nm)		λ_{max} (nm)
1	50	200	0.031	IR
2	50	150	0.049	IR
3	50	100	0.087	IR
4	50	50	0.196	IR
5	100	200	0.087	440.3
6	100	150	0.126	488.1
7	100	100	0.196	580.6
8	200	200	0.196	546.2
9	200	150	0.256	549.0

The assembly of these peptide mediated hybrid systems is shown in figure 4. In these systems, we used genetically engineered polypeptides for inorganic surfaces (GEPIs) as a fusion partner[17] to couple QDs and CCPs. GEPIs are advantageous over using organic thiolated molecules because of its biomolecular recognition for inorganic compounds, bifunctionality, and self-assembling properties. Using gold and platinum patterns on SiO_2/Si substrate, we have demonstrated the specific adsorption of gold-binding polypeptide specific onto the gold patterns and neither onto the platinum patterns nor SiO_2/Si regions.[18] In order for gold binding polypeptide to recognize and to self-assemble the CdSe-ZnS core-shell QDs ($\lambda_{em} \approx 605$ nm), we used biotin-streptavidin interaction, a widely used application for their stability and to support subsequent layer assemblies. As a nanoscale building block, streptavidin (SA) molecules

provided well-ordered homotetrametric entity with 4 binding sites, appropriate size, and high affinity for biomolecular recognition. We used commercially available streptavidin functionalized QDs. QDs circumvent the short comings of organic dyes because they have excellent photostability, a broad absorption and a narrow emission band.

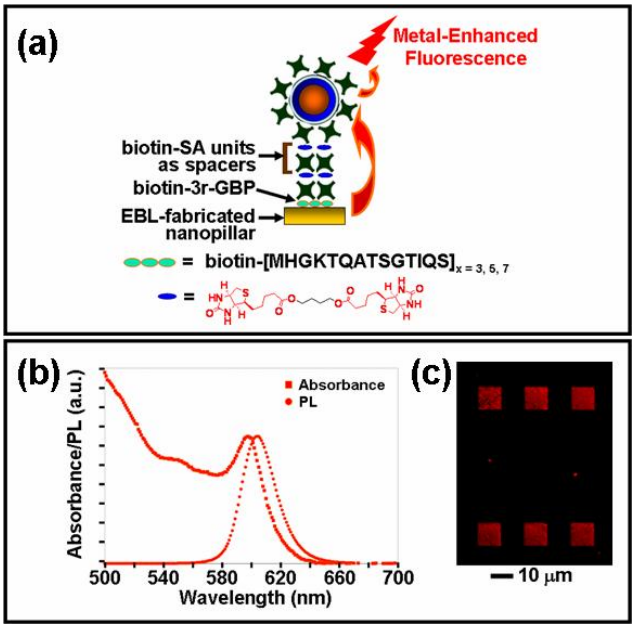

Fig 4. Biomolecular recognition-mediated fabrication of tunable QD arrays. (a) Sketch of the peptide-mediated surface-immobilized QD hybrid nanoassemblies. (b) Spectral properties of the QDs. (c) Fluorescence image of a series of QD arrays with the highest fluorescence enhancement (pattern #2.3 – D = 100 nm, d_{tt} = 100 nm, $h \approx 16$ nm); the enhancement factor was ~ 15, relative to the QD emission on a planar gold substrate after normalization over the area fill factor.

The lateral distance of the QDs nanoarrays were tuned at three different metal distances, ~8.70 nm, ~16.00 nm, and ~20.30 nm using gold binding polypeptides and biotin-streptavidin spacer units. These well-defined QD-metal distances were characterized using atomic force microscopy, figure 5 These separations positioned the QD at three spatial locations within the amplified local EM field of the gold nanopillars where the polarization strengths are believed to be different.

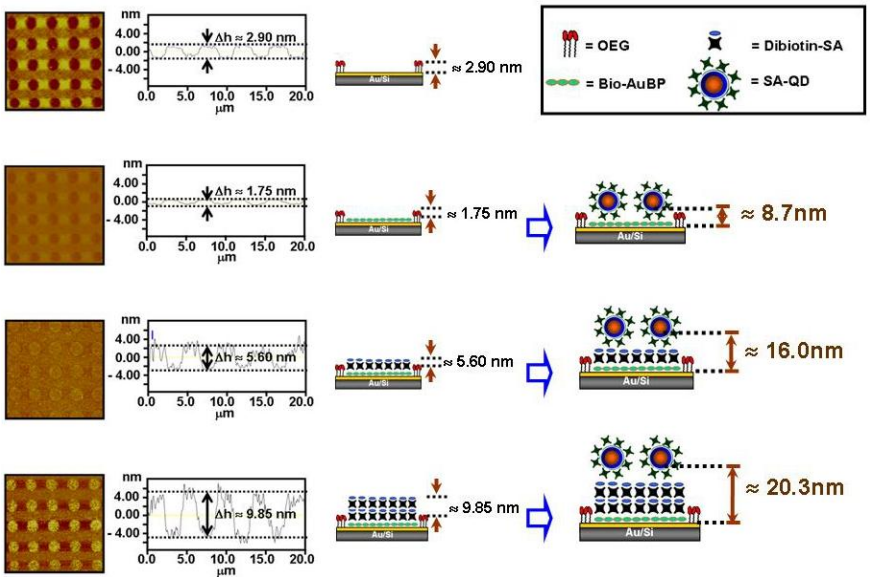

Fig. 5. AFM measurements of linker lengths. The heights of molecular linkers were experimentally measured relative to the height of OEG self-assembled monolayers. This is accomplished by backfilling of linkers into the 2-μm hole arrays generated by μCP of OEG molecules, followed by cross-sectional profile analysis to measure the relative difference in heights between patterned OEG regions and linker regions.

The QDs nanoarrays were locally excited and their emission was monitored. The photoluminescence of QD nanoarrays reveals the specificity of coupling QDs onto gold nanopillars. Figure 6 compares the area normalized photoluminescence plots of different QD nanoarrays. The emission intensity of QDs nanoarrays dramatically increased as we increased the QD-metal distance from ~8.70 nm to ~16.00 nm. Further increasing the QD-metal distance to ~20.30 nm, we observed a decrease in the QD emission. It should be noted that the QD emission at a QD-metal distance ~20.30 nm is higher than at a QD-metal distance of ~8.70 nm. This suggests that the PL quenching is a short-range effect and weakens with distance more rapidly than EM field amplification responsible for PL enhancement.[19] Similar dependence of QD emission on the separation from gold surface has been reported by Kulakovich et al. who obtained the largest fluorescence enhancements at ~11.70 nm; in the same study, it was found that the QD emission was no longer enhanced at distances greater than 25 nm.

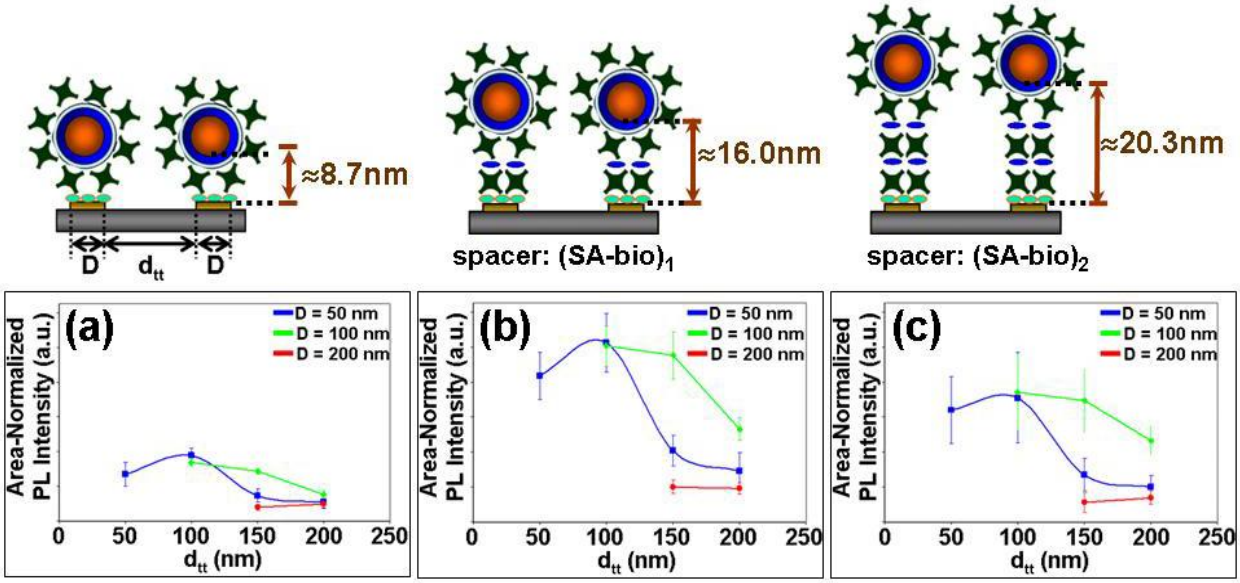

Fig. 6. Tunable QD arrays with surface-plasmon-enhanced photoluminescence. Area-normalized PL intensity from QDs in a particular pattern at different QD-metal distances of 8.7 nm (a), 16.0 nm (b) and 20.3 nm (c). Schematic illustrations show the structure of hybrid nanoassemblies.

The horizontal tuning of the localized surface plasmon resonance also played a significant role in the emission of the QDs. Of the various sizes produced, 200 nm gold nanopillars showed the least efficient for fluorescence enhancement. In addition, the emission intensities of the QDs were similar as the tip-to-tip spacing varied from 150 to 200 nm. This suggest weak optical communication in large metal nanoarrays, where nanopillars interacted with the excitation light and participated in local electric field enhancement as individual nanopillars, rather than as collective entity of strongly interacting nanopillars. Thus, the emission intensity of QDs self-assembled on 200 nm gold nanopillars was independent of the lattice spacing. These results were similar to those reported by Pompa et al. For 100 nm gold nanoarrays, we observed the opposite where the QDs emission changed as the tip-to-tip spacing changed. We also observed a dramatic increase in the fluorescence enhancement. There was a much stronger optical communication in 100 nm gold nanoarrays. It was found that the tip-to-tip distance of 100 nm appears to be the optimal separation between the particles in the QD arrays. For both 50 nm and 100 nm arrays, emission intensity was the highest at d_{tt} = 100 nm.

We observed surface plasmon enhanced fluorescence of tunable QD nanoarrays with the highest fluorescence enhancement of ~15-fold was achieved. Enhancement factors were calculated relative to self-assembling QDs on flat gold surfaces and normalized over the area fill factor. Enhancement factors shown in figure 7 revealed that the emission of the QDs was enhanced at all QD-metal distances on all gold nanoarrays.

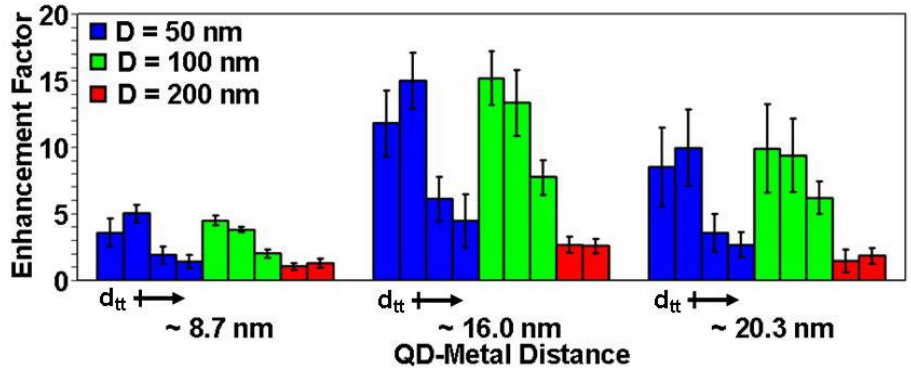

Fig. 7. Enhancement factors of the QD arrays. To ensure a reliable normalization, the distance-effect was taken into account; QDs are attached onto either gold nanopillars or planar gold substrates using the same linkers and their PL

intensities were measured. Enhancement factors were calculated by dividing the PL intensity from QDs in a particular pattern by that from QDs in an unpatterned area.

Based on the surface plasmon enhanced QD nanosystem, the lateral distance of conjugated polymer, PFDBT-N^+, was tuned at two distances, ~12.75 nm and ~18.50 nm using gold binding polypeptide as the fusion partner and biotin-streptavidin as the spacer units. The self-assembly of the CCP arrays occurs through electrostatic interactions between the positive charged PFDBT-N^+, the negatively charged phosphate backbone of DNA, and positively charged gold-binding polypeptides. PFDBT-N^+ was locally excited and the emission intensity was measured as shown in figure 8.

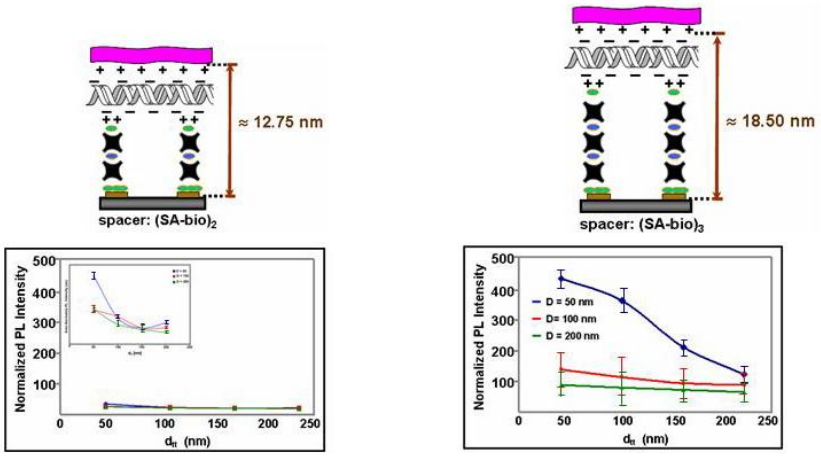

Fig. 8. Tunable conjugated polymer arrays with surface-plasmon-enhanced photoluminescence. Area-normalized PL intensity from conjugated polymers in a particular pattern at different conjugated polymer-metal distances of ~12.75 nm and ~18.50 nm. Schematic illustrations show the structure of hybrid nanoassemblies.

The emission intensity of PFDBT-N^+ dramatically increased as the CCP-metal distance increased from ~12.75 nm to ~18.50 nm. The optimum PL is observed on 50 nm gold nanoarrays where a decrease in emission intensity occurred as the tip-to-tip distance increased. These results are in agreement with experimental results of the QD nanoarray. Thus the optimum fluorophore-metal distance for fluorescence enhancement ranges from 16-19 nm.

The effects of nanopillar size and their tip-to-tip spacing on surface plasmon enhanced fluorescence revealed that 50 nm gold nanopillars were the most efficient and 200 nm the least efficient. For smaller nanoarrays, the emission intensity of PFDBT-N^+ decreased more dramatically as d_{tt} increased. In contrast, PFDBT-N^+ emission remained similar for 200 nm nanoarrays as d_{tt} increased. Thus the emission intensity of PFDBT-N^+ was dependent on smaller nanoarrays and became less apparent when self-assembled on larger nanoarrays. Thus the strong role of near-field coupling between neighboring nanopillars altered the emission of PFDBT-N^+ and suggestted a spectral relationship between the optical properties of metal nanoarrays and PFDBT-N^+. As the distance between PFDBT-N^+ and the metal surface increased to ~18.50 nm, the emission intensity of PFDBT-N^+ dramatically increased. The optimum fluorescence enhancement was observed on 50 nm gold nanoarrays where a decrease in emission intensity occurred as the tip-to-tip distance increased. It was found that the tip-to-tip distance of 50 nm appears to be the optimal separation between the particles in the CCP arrays. For both 50 nm and 100 nm arrays, emission intensity was the highest at d_{tt} = 50 nm.

Surface plasmon enhanced fluorescence of tunable CCP arrays was successfully fabricated where a 25-fold increase in PFDBT-N^+ emission was achieved. Enhancement factors were calculated relative to CCPs self-assembled on flat gold surfaces and normalized over the area fill factor. Enhancement factors shown in figure 9 revealed that the emission of PFDBT-N^+ was enhanced on all gold nanoarrays.

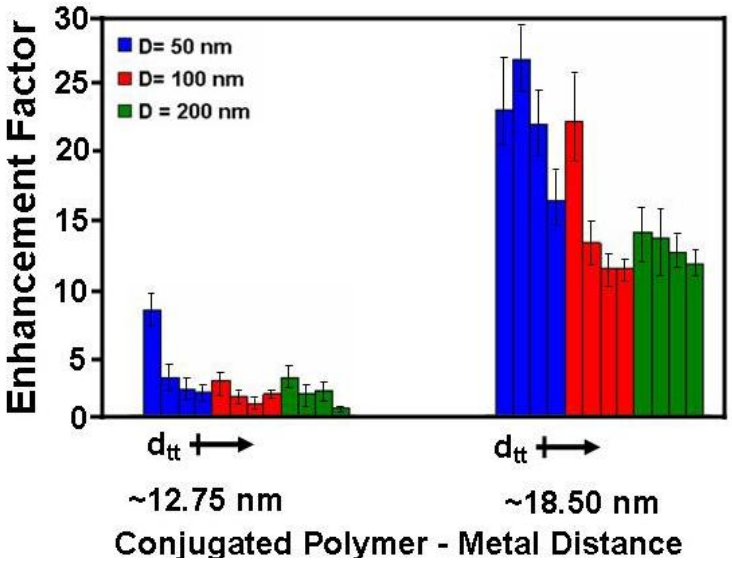

Fig. 9. Enhancement factors of the conjuagated polymer arrays. To ensure a reliable normalization, the distance-effect was taken into account; conjugated polymers are attached onto either gold nanopillars or planar gold substrates using the same linkers and their PL intensities were measured. Enhancement factors were calculated by dividing the PL intensity from conjugated polymers in a particular pattern by that from conjugated polymers in an unpatterened area.

5. CONCLUSION

We briefly discussed the potential for further optimizing the fluorescence enhancement and several key features that make our approach suitable for investigating resonance phenomena in hybrid nanostructures. Surface-plasmon-enhanced emission of up to several hundred- or thousand-fold amplifications can be expected theoretically in smartly designed systems where the spectral relationships of fluorophores and plasmonic structures are properly tuned. Our approach provides an independent optimization of fluorophores (through colloidal synthesis), plasmonic template (through lithographic patterning) as well as the emitter-metal distance (through step-wise self-assembly), thereby opening up unlimited possibilities to create optimally integrated systems for the target application. Moreover, simply improving the quantum yield (as high as 90%) of QDs and conjugated polymers could increase the fluorescence enhancement. A synergetic combination of inorganic nanostructures, biomolecular recognition-mediated assembly, and lithographic patterning should enable the precise control necessary to produce highly integrated multifunctional hybrid nanoassemblies on all length scales for a diverse range of nanobiotechnological applications.

ACKNOWLEDGEMENTS

This research was supported partially by the Bioinspired Materials and Systems Program through the Air Force Office of Scientific Research (US-AFOSR), UW-DURINT (Defense University Research Initiative on Nanotechnology) through the Army Research Office (US-ARO), and the GEMSEC (Genetically Engineered Materials Science and Engineering Center) through NSF-MRSEC program. A. K-Y. Jen thanks the Boeing-Johnson Foundation for its support. M. T. Zin thanks the Center for Nanotechonolgy for its support. Instrumentation for electron-beam lithography was provided by the Nanotechnology User Facility (NTUF), a member of the National Nanotechnology Infrastructure (NNIN) supported by NSF.

REFERENCES

[1] (a) Niemeyer, C. M. *Angew. Chem. Int. Ed.* **2001**, *40*, 4128-4158; *Angew. Chem.* **2001**, *113*, 4254-4287. (b) Dujardin, E.; Mann, S. *Adv. Mater.* **2002**, *14*, 775-788. (c) Seeman, N. C.; Belcher, A. M. *Proc. Natl. Acad. Sci. U.S.A.*, **2002**, *99*, 6452-6455. (d) Sarikaya, M. *Proc. Natl. Acad. Sci. U.S.A.* **1999**, *96*, 14183-14185.

[2] (a) Lee, J.; Govorov, A. O.; Dulka, J.; Kotov, N. A. *Nano Lett.* **2004**, *4*, 2323-2330. (b) Oh, E.; Hong, M.-Y.; Lee, D.; Nam, S.-H.; Yoon, H. C.; Kim, H.-S. *J. Am. Chem. Soc.* **2005**, *127*, 3270-3271.

[3] (a) Gattás-Asfura, K.M.; Zheng, Y.; Micic, M.; Snedaker, M.J.; Ji, X.; Sui, G.; Orbulescu, J.; Andreopoulos, F.M.; Pham, S.M.; Wang, C., and Leblanc, R.M., *J. Phys. Chem. B,* **2003**, 107, 10464 -10469. (b) Zin, M.T.; Munro, A.M.; Gungormus, M.; Wong, N.-Y.; Ma, H.; Tamerler, C.; Ginger, D.S.; Sarikaya, M., and Jen, A.K.-Y., *J. Mater. Chem*., **2007**, 17, 866–872. (c) Zhang, C.-Y.; Yeh, H.-C.; Kuroki, M.T., and Wang, T.-H., *Nature Materials*, **2005**, 4, 826-831.
[4] Sosa, I. O.; Noguez, C., and Barrera, R.B., *J. Phys. Chem. B,* **2003**, 107, 6269 -6275.
[5] Lakowicz, J.R*., Anal Biochem,* **2001**, 298, 1-24.
[6] Lakowicz, J.R. *Principles of Fluorescence Spectroscopy*, 2nd ed.; Kluwer/Plenum L New York, 1999.
[7] Haes and Van Duyne *MRS Bulletin,* **2005**, 30, 368-375.
[8] Chana, W.C.W.; Maxwell, D.J.;Gaob, X.; Bailey, R.E.;Hanc,M.,and Nie, S., *Current Opinion in Biotechnology,* **2002**, 13, 40-46.
[9] McQuade, D.T.; Pullen, A.E., and Swager, T.M., *Chem. Rev.* **2000,** *100,* 2537-2574.
[10] Dai, L.; Soundarrajan, P. and Kim, T, *Pure Appl. Chem.,* **2002,** 74, 1753–1772.
[11] (a) Tyagi, S.; Kramer, F. R. *Nat. Biotechnol.* **1996**, *14*, 303-308. (b) Heyduk, T.; Heyduk, E. *Nat. Biotechnol.* **2002**, *20*, 171-176. (c) Fang, X.; Li, J. J.; Tan, W. *Anal. Chem.* **2002**, *72*, 3280-3285. (d) Alberts, D. P.; Parman, J. M.; Goddard, N. L. *Biophys. J.* **2003**, *84*, 3212-3217. (e) Antony, T.; Thomas, T.; Sigal, L. H.; Shirahata, A.; Thomas, T. J. *Biochemistry* **2001**, *40*, 9387-9395. (f) Bonnet, G.; Tyagi, S.; Libchaber, A.; Kramer, F. R. *Proc. Natl. Acad. Sci. U.S.A*. **1999**, *96*, 6171-6176. (g) Dubertret, B.; Calame, M.; Libchaber, A. J. *Nat. Biotechnol.* **2001**, *19*, 365-370.
[12] Lidstrom, M.E.; Meldrum, D.R., *Nature Reviews* **2003**, 1, 158-164.
[13] (a) Neumann, T.; Johansson, M.-L.; Kambhampati, D.; Knoll, W. *Adv. Funct. Mater.* **2002**, *12*, 575-586. (b) Liermann, T.; Knoll, W.; Sluka, P.; Herrmann, R. *Colloids Surf. A* **2000**, *169*, 337-350.
[14] Bohren, C. F.; Huffman, D. R. *Absorption and Scattering of Light by Small Particles*; Wiley: New York, 1983.
[15] (a) Mock, J. J.; Barbic, M.; Smith, D. R.; Schultz, D. A.; Schultz, S. *J. Chem. Phys.* **2002**, *116*, 6755-6759. (b) Sherry, L. J.; Chang, S.-H.; Schatz, G. C.; Van Duyne, R. P.; Wiley, B. J.; Xia, Y. *Nano Lett.* **2005**, *5*, 2034-2038. (c) Nehl, C. L.; Liao, H.; Hafner, J. H. *Nano Lett.* **2006**, *6*, 683-688. (d) Langhammer, C.; Yuan, Z.; Zoric, I.; Kasemo, B. *Nano Lett.* **2006**, *6*, 833-838.
[16] Kelly, K. L.; Coronado, E.; Zhao, L. L.; and George C. Schatz *J. Phys. Chem. B* **2003**, 107, 668-677.
[17] Meier, M.; Wokaun, A.; Liao, P. F. *J. Opt. Soc. Am. B* **1985**, *2*, 931-949.
[18] (a) Sarikaya, M.; Tamerler, C.; Jen, A. K.-Y.; Schulten, K.; Baneyx, F. *Nature Mater.* **2003**, *2*, 577-585. (b) Sarikaya, M.; Tamerler, C.; Schwartz, D. T.; Baneyx, F. *Annu. Rev. Mater. Res.* **2004**, *34*, 373-408.
[19] Stewart, M. E.; Anderton, C. R.; Thompson, L. B.; Maria, J.; Gray, S. K.; Rogers, J. A. and Nuzzo, R. G., *Chem. Rev*. **2008**, 108, 494-521.